Published in final edited form as:
Cell Rep. 2013 April 25; 3(4): 1164–1174. doi:10.1016/j.celrep.2013.03.028.

p21 Both Attenuates and Drives Senescence and Aging in BubR1 Progeroid Mice

Darren J. Baker[1], **Robbyn L. Weaver**[2], and **Jan M. van Deursen**[2,*]

[1]Department of Pediatric and Adolescent Medicine Mayo Clinic College of Medicine, Rochester, MN 55905, USA

[2]Department of Biochemistry and Molecular Biology Mayo Clinic College of Medicine, Rochester, MN 55905, USA

SUMMARY

BubR1 insufficiency occurs with natural aging and induces progeroid phenotypes in both mice and children with mosaic variegated aneuploidy syndrome. In response to BubR1 insufficiency, skeletal muscle, fat, and lens tissue engage $p19^{Arf}$ to attenuate senescence and age-related deterioration. Here, we address how $p19^{Arf}$ exerts this caretaker role using BubR1 progeroid mice lacking *p53* or its transcriptional target *p21*. We show that p53 delays functional decline of skeletal muscle and fat in a p21-dependent fashion by inhibiting $p16^{Ink4a}$-mediated senescence of progenitor cells. Strikingly, p53 also attenuates the formation of cataractous lenses, but here its antiaging effect is p21 independent, as we found p21 to promote senescence of lens epithelial cells and cataract formation. Together, these results demonstrate that p53 counteracts tissue destruction in response to BubR1 insufficiency through diverse mechanisms and uncover a causal link between senescence of the progenitor cell compartment and age-related dysfunction.

INTRODUCTION

Aging is a complex biological process that increases the risk of a broad spectrum of human diseases and disorders, including diabetes, osteoporosis, arthritis, cataracts, sarcopenia, and cardiovascular and neurological disease (Campisi, 2005; Gau et al., 2011; Lotz and Caramés, 2011). Despite the importance of aging to human health, the molecular mechanisms underlying the progressive physiologic decline with aging remain incompletely understood (Marion et al., 2009). Studies in animal model systems have identified various genes that promote longevity when mutated, including genes that encode components of key metabolic pathways (Kenyon, 2010). Other efforts to understand how we age focus on genes associated with human progeria syndromes or mouse models that develop features resembling accelerated aging (Burtner and Kennedy, 2010). One of these genes encodes for BubR1, a core component of the mitotic checkpoint that ensures accurate segregation of chromosomes by participating in the inhibition of the ubiquitin E3 ligase activity of Cdc20-activated anaphase-promoting complex in the presence of unattached chromosomes (Baker et al., 2004). Mutant mice carrying *BubR1* hypomorphic alleles (referred to as $BubR1^{H/H}$ mice) that produce low amounts of the protein develop multiple progeroid and aging-associated phenotypes, including short lifespan, dwarfism, facial dysmorphisms, cataracts, sarcopenia, (subdermal) fat loss, impaired wound healing, and reduced dermal thickness

*Correspondence: vandeursen.jan@mayo.eduhttp://dx.doi.org/10.1016/j.celrep.2013.03.028.

SUPPLEMENTAL INFORMATION Supplemental Information includes four figures and can be found with this article online at http://dx.doi.org/10.1016/j.celrep.2013.03.028.

(Baker et al., 2004, 2008a; Hartman et al., 2007; Matsumoto et al., 2007). Mutations in human *BubR1* are associated with mosaic variegated aneuploidy (MVA), a rare syndrome that is characterized by aneuploidization and various progeroid traits, including short lifespan, short stature, cataracts, facial dysmorphisms, and mental retardation (Hanks et al., 2004; Lane et al., 2002; Matsuura et al., 2006; Suijkerbuijk et al., 2010). Several of these age-associated features are observed in mice carrying a monoallelic *BubR1* MVA mutation (Wijshake et al., 2012). Furthermore, BubR1 levels decrease with age in various mouse tissues and sustained overexpression of BubR1 extends mouse healthspan and lifespan, which has prompted speculation that BubR1 might be a determinant of chronological aging (Baker et al., 2004, 2013; Hartman et al., 2007; Matsumoto et al., 2007).

$p16^{Ink4a}$ and $p19^{Arf}$, two biomarkers of human and rodent aging (Krishnamurthy et al., 2004), are selectively induced in skeletal muscle, fat, and eye tissue of BubR1 progeroid mice (Baker et al., 2008b). Genetic inactivation of *p16*^{Ink4a} or clearance of $p16^{Ink4a}$-positive cells from BubR1 progeroid mice slows functional decline of these tissues, demonstrating a causal link between accumulation of senescent cells and functional impairment in these tissues (Baker et al., 2008a, 2008b, 2011), although the types of cells that are senescing have not been defined. Inactivation of *p19*^{Arf}, on the other hand, accelerates sarcopenia, fat loss, and cataract formation, implying that its induction in response to BubR1 insufficiency acts to suppress cellular stress that drives cells into a senescent state (Baker et al., 2008b). $p19^{Arf}$ accumulates in the nucleolus, where it binds NPM1 and Mdm2 to suppress tumor development by inhibiting ribosome biogenesis and initiating p53-dependent senescence and apoptosis, respectively (Conboy et al., 2003; Conboy and Rando, 2002; Kamijo et al., 1997). The recent discovery of additional binding partners has alluded to the existence of various p53-in-dependent cellular functions of $p19^{Arf}$ (Conboy et al., 2003; Rio Frio et al., 2010). The hypothesis that $p19^{Arf}$ might exert its anti-progeroid effects in the context of BubR1 insufficiency through a p53-dependent mechanism is directly challenged by studies onother progeroid mouse strains, such as *Zmpste24* null (a model for Hutchinson-Gilford progeria), *Brca1* null, and *Ercc1* hypomorphic mice, showing that p53 drives early aging in these models (Cao et al., 2003; Kirkwood, 2002; Maier et al., 2004; Núñez et al., 2000; Sharpless, 2004; Tyner et al., 2002; Varela et al., 2005).

Here, we further explored the molecular basis of MVA syndrome and the potential multifaceted role of p53 in premature aging using p53-deficient BubR1 hypomorphic mice. p53 has hundreds of potential downstream target genes implicated in a wide variety of biological processes, including transient cell-cycle arrest, cellular senescence, apoptosis, inhibition of angiogenesis, autophagy, metabolism, and DNA repair (el-Deiry, 1998; Nakamura, 2004; Papazoglu and Mills, 2007). However, the impact of individual p53 target genes on (accelerated) aging remains largely unknown. We focused on the role of *p21*, a p53 target gene implicated in cell-cycle arrest and cellular senescence (Cheung et al., 2012; Vousden and Prives, 2009), using BubR1 hypomorphic mice that we bred onto a *p21* null genetic background. In addition to revealing that p53 is the critical mediator of the $p19^{Arf}$-induced antiaging responses in BubR1 progeroid mice, we identify *p21* as the key downstream p53 target gene through which the p53 protector function is executed in two tissues: skeletal muscle and fat. Interestingly, we find that insufficiency of BubR1 induces several senescence-associated markers in progenitor cells residing in these tissues, not in terminally differentiated cells. Senescence of these progenitors is further elevated upon deletion of *p21*, demonstrating that activation of p53 in BubR1 hypomorphic mice acts to mobilize antiaging responses in adipose and skeletal muscle tissue. Furthermore, we find that p21 induction in lens tissue promotes cataract formation, but that p21-independent p53 responses counteract this p21 effector function. These findings indicate that BubR1 insufficiency elicits an aging response that is counteracted by p53 and involves single or multiple p53 targets, depending on the tissue type.

RESULTS

p53 and p21 Activation in *BubR1*$^{H/H}$ Mice Acts to Extend Lifespan

p19^{Arf} has several diverse functions, one of which is to stabilize p53 through inhibition of Mdm2 (Conboy et al., 2003). Since p53 has been linked to senescence and aging, we sought to determine whether the p19^{Arf}-dependent antiaging mechanism activated in response to BubR1 insufficiency involves p53. As a first step, we analyzed skeletal muscle, fat, and eye from 2-month-old *BubR1*$^{H/H}$ and wild-type mice for p53 protein levels by western blot analysis. Previously, we documented that p19^{Arf} expression is markedly increased in these three tissues (Baker et al., 2008b). Fat and eye extracts of *BubR1*$^{H/H}$ mice indeed contained elevated levels of p53 protein (Figure 1A). We found that the p53 target p21 was also elevated in these same tissues (Figure 1A). Western blots of skeletal muscle extracts probed for p53 and p21 were inconclusive (data not shown), but quantitative RT-PCR (qRT-PCR) analysis demonstrated that *p21* gene transcript levels were significantly increased in skeletal muscle of *BubR1*$^{H/H}$ mice (Figure 1B), suggesting that p19^{Arf} induction resulted in p53 stabilization in this tissue as well. *BubR1*$^{H/H}$ tissues that developed age-related pathology in a p19^{Arf}-independent fashion (i.e., brain and aorta) or had no age-related phenotypes (i.e., lung, pancreas, and colon) did not exhibit increased expression of *p21* (Figure S1). Thus, p53 and p21 appear to be selectively induced in p19^{Arf}-positive *BubR1*$^{H/H}$ tissues subjected to premature aging.

To determine the role of p53 and p21 in the p19^{Arf}-dependent antiaging mechanism activated in response to BubR1 insufficiency, we bred *BubR1*$^{H/H}$ mice onto a *p*53 (Jacks et al., 1994) or *p21* (Brugarolas et al., 1995) homozygous null genetic background. Cohorts of *BubR1*$^{H/H}$, *p53*$^{-/-}$, and *p21*$^{-/-}$ mice were used as controls. All cohorts were monitored for the development of age-related phenotypes for a period of up to 1 year. Ablation of *p53* or *p21* dramatically shortened the median overall survival of *BubR1*$^{H/H}$ mice by 35% (Figure 1C). Additionally, the maximum lifespan of *BubR1*$^{H/H}$;*p53*$^{-/-}$ or *BubR1*$^{H/H}$;*p21*$^{-/-}$ mice was significantly decreased compared to *BubR1*$^{H/H}$ mice (Figure 1C). The tumor incidence of *BubR1*$^{H/H}$;*p53*$^{-/-}$ mice was low compared to that of *p53*$^{-/-}$ mice, with 17% of *BubR1*$^{H/H}$;*p53*$^{-/-}$ mice having tumors compared to 96% of *p53*$^{-/-}$ mice (Figure 1D). Although the overall tumor latency (thymic lymphoma and osteosarcoma) was similar for *BubR1*$^{H/H}$; *p53*$^{-/-}$ and *p53*$^{-/-}$ mice (Figure 1E), the latency of osteosarcoma of *BubR1*$^{H/H}$;*p53*$^{-/-}$ mice was significantly decreased, indicating that BubR1 insufficiency accelerates sarcoma formation in the absence of p53 (Figure 1D). No tumors were observed upon postmortem examination of *BubR1*$^{H/H}$;*p21*$^{-/-}$ mice (Figure 1D). These data reveal that the substantial reduction in lifespan of BubR1 hypomorphic animals lacking p53 or p21 cannot be explained by accelerated tumorigenesis.

p53 Acts through p21 to Delay Progeroid Decline in Muscle and Fat

Inactivation of *p19*^{Arf} accelerates sarcopenia, fat loss, and cataract formation in *BubR1*$^{H/H}$ mice. If *p53* and *p21* inactivation phenocopy the effects of *p19*^{Arf} depletion, this would indicate that p53 would be the critical target of p19^{Arf}, and p21 that of p53. Consistent with this, we found that lordokyphosis (an abnormal rearward curvature of spine), a phenotype that in *BubR1*$^{H/H}$ mice is caused by sarcopenia (Baker et al., 2004), was significantly accelerated in both *BubR1*$^{H/H}$;*p53*$^{-/-}$ and *BubR1*$^{H/H}$; *p21*$^{-/-}$ mice (Figure 2A). Gastrocnemius and abdominal muscles of 6-week-old *BubR1*$^{H/H}$;*p53*$^{-/-}$ and *BubR1*$^{H/H}$;*p21*$^{-/-}$ mice had significantly smaller fibers than those of *BubR1*$^{H/H}$ mice (Figure 2B), confirming that sarcopenia was indeed accelerated following the loss of p53 or p21. Lordokyphosis did not develop in *p53*$^{-/-}$ and *p21*$^{-/-}$ mice during the 1 year observation period (data not shown). Skinning of 6-week-old mice demonstrated that adipose tissue deposits of *BubR1*$^{H/H}$;*p53*$^{-/-}$ and *BubR1*$^{H/H}$; *p21*$^{-/-}$ mice were overtly smaller than those of

BubR1$^{H/H}$ mice (Figure 2C). The weight of the inguinal adipose tissue (IAT) revealed that this fat depot was significantly reduced (Figure 2D). Consistent with reduced fat and muscle volume, *BubR1*$^{H/H}$; *p53*$^{-/-}$ and *BubR1*$^{H/H}$;*p21*$^{-/-}$ mice had significantly lower body weights than *BubR1*$^{H/H}$ mice (Figure 2D). The progeroid phenotypes of dermal thinning and arterial wall stiffening were not exacerbated following the loss of *p53* or *p21* (Figures S2A and S2B), which is consistent with the finding that *p21* levels are not elevated in dermis and aorta of *BubR1*$^{H/H}$ mice (Figure S1). Collectively, these data provide evidence that induction of p21 through p19^{Arf}-dependent stabilization of p53 counteracts aging-associated functional decline of skeletal muscle and fat tissue in response to BubR1 insufficiency.

p21 Inhibits Degeneration of Skeletal Muscle and Fat by Preventing Senescence

To provide insight into the mechanism by which *p21* inactivation promotes functional decline of skeletal muscle and fat tissue of BubR1 hypomorphic mice, we asked if loss of *p53* or *p21* acts to promote cellular senescence, a process that has been linked to age-related pathologies in this model (Baker et al., 2008b, 2011). Fat of 5-month-old prematurely aged *BubR1*$^{H/H}$ mice is known to express high amounts of senescence-associated β-galactosidase (SA-β-gal), an established marker for the detection of senescent cells in cell culture and select mouse tissues (Baker et al., 2008b, 2011). Adipose tissue of *BubR1*$^{H/H}$ mice showed relatively low SA-β-gal activity at 6 weeks of age. In contrast, fat of *BubR1*$^{H/H}$;*p53*$^{-/-}$ and *BubR1*$^{H/H}$;*p21*$^{-/-}$ mice showed high SA-β-gal activity at this age (Figure 3A), indicating increased senescence. In keeping with this, other markers of cellular senescence in fat were also markedly elevated, including *p16*^{Ink4a}, *p19*^{Arf}, *Pai1*, *Igfbp2*, and *IL-6* (Baker et al., 2008b, 2011; Krishnamurthy et al., 2004) (Figure 3B). Similarly, markers of skeletal muscle senescence, such as *p16*^{Ink4a}, *p19*^{Arf}, *Igfbp2*, *Mmp13*, and *Nrg1* (Baker et al., 2008b), were all elevated in *BubR1*$^{H/H}$ muscles compared to wild-type muscles, and even more in *BubR1*$^{H/H}$;*p53*$^{-/-}$ and *BubR1*$^{H/H}$;*p21*$^{-/-}$ muscles (Figure 3C). Cell proliferation, as measured using in vivo BrdU incorporation, was considerably lower in both adipose tissue and skeletal muscle of *BubR1*$^{H/H}$;*p53*$^{-/-}$ and *BubR1*$^{H/H}$;*p21*$^{-/-}$ mice than in *BubR1*$^{H/H}$ mice (Figure 3D), further supporting the notion that rates of senescence were increased in these tissues. In accordance with previous observations (Baker et al., 2004, 2008a), the premature aging of these tissues is not associated with increased DNA damage (Figures S2C and S2D). We note that the attenuating effect of p53 or p21 on in vivo senescence in *BubR1*$^{H/H}$ mice cannot be recapitulated in vitro using cultured *BubR1*$^{H/H}$ mouse embryonic fibroblasts (MEFs), most likely because these cells immortalize when *p53* or *p21* is lacking (Figures S2E–S2H). Collectively, the above data suggest that p53-mediated activation of *p21* in response to BubR1 insufficiency acts to preserve skeletal muscle and adipose tissue integrity by driving cells into a state of reversible temporal cell-cycle arrest that protects against entry into a senescent state.

p21 Attenuates Progenitor Cell Senescence in Muscle and Fat of *BubR1*$^{H/H}$ Mice

Although accumulation of senescent cells in skeletal muscle and fat of *BubR1*$^{H/H}$ mice has been causally implicated in tissue dysfunction, the types of cells in these tissues that are subject to senescence were unknown. To address these key open questions, IAT collected from 5-month-old *BubR1*$^{H/H}$ mice was stained for SA-β-gal, squeezed between two microscopy slides, and analyzed by light microscopy. While mature adipocytes were negative for SA-β-gal, areas that appeared to track with the fat tissue vasculature were frequently positive (Figure 4A). These areas include endothelial cells, white blood cells, adipocyte stem cells (ASCs), and preadipocytes (PACs), collectively termed the stromal vascular fraction (SVF) (Cawthorn et al., 2012). To determine which cells of the SVF were prone to senescence, we prepared single cells from IAT using collagenase treatment and a combination of centrifugation and fluorescence-activated cell sorting to collect mature adipocytes, endothelial cells, and a combined population of ASCs and PACs (Figure S3A).

As expected, mature adipocytes stained negative for SA-β-gal, whereas the SVF was highly positive (Figure S3B). Strikingly, the relative number of ASCs/PACs in the SVF of 2-month-old *BubR1*$^{H/H}$ mice was about 3-fold lower than in wild-type mice (Figure 4B). Compared to wild-type mice, *p16*^{Ink4a} transcript levels were highly elevated in the ASC/PAC cell fraction of *BubR1*$^{H/H}$ mice, but not in adipocytes and endothelial cells (Figure 4C). Other markers of cellular senescence were also markedly elevated in this fraction (Figure 4D), indicating that fat progenitor cells with low amounts of BubR1 are prone to become senescent.

Senescent cells in skeletal muscle of *BubR1*$^{H/H}$ mice do not visibly stain the tissue for SA-β-gal activity (data not shown), precluding microscopy as a means to provide insight into the kinds of cells in this tissue that are prone to senescence. In an alternative approach outlined in Figure S3C, we used collagenase treatment of skeletal muscle from 2-month-old *BubR1*$^{H/H}$ mice followed by purification of muscle fibers and particular populations of mononuclear cells, including quiescent satellite cells (Q-SCs; muscle stem cells) and fibro/adipogenic progenitors (FAPs; a subpopulation of mononuclear cells that does not generate myofibers but facilitate myogenesis; Joe et al., 2010). Mature skeletal muscle fibers from *BubR1*$^{H/H}$ mice exhibited no significant increase in *p16*^{Ink4a} transcripts (Figure 5A), nor did Q-SCs from these mice. In contrast, the FAP pool of *BubR1*$^{H/H}$ cells had very high *p16*^{Ink4a} transcript levels compared to their counterparts from wild-type mice (Figure 5A). Several additional markers of senescence in skeletal muscle were elevated in the FAP population (Figure 5B), indicating that progenitor cells with insufficient amounts of BubR1 are prone to senesce.

We next collected ASC/PAC and FAP populations from *BubR1*$^{H/H}$;*p21*$^{-/-}$ mice to examine whether accelerated aging in the skeletal muscle and fat of these animals correlates with increased progenitor cell senescence. All markers of senescence were significantly higher in ASCs/PACs from *BubR1*$^{H/H}$;*p21*$^{-/-}$ mice than from *BubR1*$^{H/H}$ (Figure 4D). FAP populations also exhibited an even further elevation in senescence markers upon loss of p21 in *BubR1*$^{H/H}$ (Figure 5B). Importantly, consistent with impaired function of FAPs, repair of cardiotoxin-induced damage of skeletal muscle tissue was already markedly impaired in *BubR1*$^{H/H}$;*p53*$^{-/-}$ and *BubR1*$^{H/H}$;*p21*$^{-/-}$ mice at a very young age (Figure 5C). Together, these data suggest that p21, through p53 activation, acts to protect progenitor cells from senescence due to BubR1 insufficiency in adipose and skeletal muscle tissue.

p53 Inhibits Cataractogenesis in *BubR1*$^{H/H}$ Mice via a p21-Independent Mechanism

A prominent aging-related feature of BubR1 hypomorphic mice is the development of cataracts (Baker et al., 2004), a phenotype that is significantly accelerated following the loss of p19^{Arf} (Baker et al., 2008b). We found that ablation of *p53* accelerated cataract formation in *BubR1*$^{H/H}$ mice (Figure 6A), which suggested that p19^{Arf}-mediated induction of p53 delayed age-related deterioration of lens tissue in a manner similar to that observed in skeletal muscle and fat. However, unlike in skeletal muscle and fat, the p53-dependent protective mechanism in lens was p21 independent, as genetic inactivation of *p21* in *BubR1*$^{H/H}$ mice resulted in delayed rather than exaggerated cataract formation (Figure 6A). To examine the potential mechanisms underlying these contrasting observations, we performed a histological assessment on lenses of 2-month-old wild-type, *BubR1*$^{H/H}$, *BubR1*$^{H/H}$; *p53*$^{-/-}$, and *BubR1*$^{H/H}$;*p21*$^{-/-}$ mice. As previously documented (Baker et al., 2004), 2-month-old *BubR1*$^{H/H}$ mice show signs of early cataract formation, with lens epithelial cells and Morgagnian globules accumulating at the posterior part of the lens (Figures 6B and 6C). In *BubR1*$^{H/H}$;*p53*$^{-/-}$ mice, these two pathological features were substantially worsened, which closely correlated with the earlier onset of cataracts in these animals. On the other hand, epithelial cells in the posterior of the lens were significantly reduced in *BubR1*$^{H/H}$;*p21*$^{-/-}$ mice and Morgagnian globules were rarely detected. Recent

findings using an INK-ATTAC transgenic construct that allows for clearance of $p16^{Ink4a}$-positive senescent cells have shown that these cells are causally implicated in cataract formation in *BubR1*$^{H/H}$ mice (Baker et al., 2011). Consistent with an accelerated rate of senescence-dependent cataract formation, *p16*^{Ink4a} transcript levels in eyes of 6-week-old *BubR1*$^{H/H}$;*p53*$^{-/-}$ mice were significantly higher than those eyes of age-matched *BubR1*$^{H/H}$ mice (Figure 6D). A very similar increase was observed for the senescent cell marker *p19*^{Arf} (Figure 6D). Furthermore, in accordance with decreased cataract formation due to prevention of cellular senescence, eyes of *BubR1*$^{H/H}$;*p21*$^{-/-}$ mice had significantly lower *p16*^{Ink4a} and *p19*^{Arf} transcript levels than eyes of *BubR1*$^{H/H}$ mice (Figure 6D). Collectively, these data provide evidence for a tissue in which p53 acts both as an effector and an attenuator of age-related deterioration through engagement of p21-dependent and p21-independent mechanisms, respectively. We found that transcript levels of multiple effectors of p53-mediated apoptosis were significantly elevated in cataractous lenses of *BubR1*$^{H/H}$ (Figure 6E), suggesting that apoptosis is a key p21-independent mechanism through which p53 attenuates cataractogenesis in *BubR1*$^{H/H}$ mice.

DISCUSSION

p19^{Arf} expression markedly increases with age in various human and rodent tissues (Krishnamurthy et al., 2004), but whether and how this tumor suppressor influences aging-related processes remains unclear. A key barrier has been the fact that *p19*^{Arf} knockout mice die of cancer before they develop age-related pathologies (Kamijo et al., 1997). In a previous study, we bypassed this problem by studying the impact of *p19*^{Arf} disruption in BubR1 progeroid mice, which revealed that $p19^{Arf}$ protects the skeletal muscle, adipose tissue, and eye of these mice against aging-related deterioration (Baker et al., 2008b). Here, we used a genetic approach involving *p53* and *p21* knockout mice to dissect the molecular mechanisms underlying this protective effect, which led to four significant insights.

First, our observation that *BubR1*$^{H/H}$;*p53*$^{-/-}$ mice phenocopy *BubR1*$^{H/H}$;*p19*$^{Arf-/-}$ mice demonstrates that p53 is the key critical downstream target of $p19^{Arf}$. In turn, our discovery that the skeletal muscle and fat phenotypes of *BubR1*$^{H/H}$;*p21*$^{-/-}$ mice mimic those of *BubR1*$^{H/H}$;*p53*$^{-/-}$ mice reveals that *p21* is the relevant target of p53 in these tissues. Both of these findings are remarkable given that $p19^{Arf}$ has a myriad of binding partners implicated in diverse biological processes (Conboy et al., 2003) and that p53 has hundreds of potential transcriptional targets as well as a growing number of nontranscriptional functions (Vousden and Prives, 2009).

Second, it has been reported that p21 drives cellular senescence and age-related pathology in a progeroid mouse model for telomere dysfunction (Choudhury et al., 2007). Our finding here that p21 loss accelerates skeletal muscle and fat deterioration in BubR1 progeroid mice uncovers a role for p21 as an attenuator of age-related decline. We show that engagement of *p21* in these tissues reduces formation of $p16^{Ink4a}$-positive senescent cells, suggesting that p21-mediated temporary cell-cycle arrest or quiescence helps relieve the stress or damage that stimulates the $p16^{Ink4a}$-Rb pathway to establish the senescent phenotype. Studies in cultured cells revealed that p21-independent p53 activities, including p53-mediated inhibition of the mTOR pathway, counteract p21-mediated cellular senescence (Minagawa et al., 2011). However, in the context of BubR1 insufficiency, the senescence suppressive effect seems entirely p21 dependent because *p21* and *p53* loss phenocopy each other in most tissues. In preliminary studies, BubR1 progeroid mice fed a diet containing the mTOR inhibitor rapamycin developed age-related phenotypes at similar rates as mice on a control diet (T.W. and J.v.D., unpublished data), which is consistent with the notion that p21-mediated protection of skeletal muscle and fat against progeroid decline does not involve p21-independent activities of p53.

Third, the observation that disruption of *p21* in BubR1 progeroid mice attenuates cataract formation provides evidence that p21 can also act as an effector of age-related deterioration in response to BubR1 insufficiency in a tissue-selective manner (Figure S4). The most straightforward explanation would be that the extent or duration of p21 engagement in lens epithelial cells reaches a threshold for activation of the senescence program, but not in skeletal muscle and fat. Intriguingly, in contrast to loss of *p21*, loss of *p53* accelerates cataract formation in BubR1 progeroid mice, characterizing p53 as a protector of age-related decline of lens tissue (Figure S4). A possible explanation for these contrasting effects would be that p21-independent functions of p53 induce apoptosis of damaged cells, thereby preventing the accumulation of cells in the posterior part of the lens where they are able to distort its integrity. This possibility is supported by the observation that several p53 target genes that mediate apoptosis are induced in lens epithelial cells in response to BubR1 insufficiency (Figure 6E). It is important to note that p53 has multiple activities other than mediating senescence and apoptosis (Vousden and Prives, 2009). Perhaps one or more of these activities may act to facilitate proper terminal differentiation of lens epithelial cells from BubR1 progeroid mice, which would also reduce the incidence of aberrant migration of lens epithelial cells to posterior part of the lens (Figure S4).

Fourth, the cell types within skeletal muscle and fat of BubR1 hypomorphic mice that undergo senescence to drive progeroid tissue dysfunction were unknown. Here, we provide evidence to suggest that progenitor cells in both these tissues are highly prone to cellular senescence. We propose that the acquisition of senescence in these cell populations may contribute to aging of the tissue through two distinct mechanisms. First, senescence acts to reduce the number of progenitors capable of undergoing the remaining steps to terminal differentiation to replenish or repair tissue. Second, these senescent progenitors may promote further dysfunction of neighboring progenitor and stem cells by affecting the niche where these cells reside through the senescence-associated secretory phenotype (SASP) that senescent cells acquire. The finding that deletion of *p21* increases senescence marker levels in progenitor populations of BubR1 hypomorphic mice suggests that p21 engagement ameliorates senescence-causing stress resulting from BubR1 insufficiency in these cells. One possibility is that these highly mitotic populations engage p21 as a molecular switch to remain in the cell cycle, rather than permanently withdrawing and producing a SASP. Earlier, we documented that the attenuating effect of $p19^{Arf}$ ablation on in vivo senescence in skeletal muscle and fat of $BubR1^{H/H}$ mice is not recapitulated by the effect on in vitro senescence in $BubR1^{H/H}$ MEFs (Baker et al., 2008b). We find that the same holds true for ablation of *p53* or *p21* (Figures S2E–S2H), underscoring that the endogenous cell signaling circuitry dictating cell fate is complex and difficult to mimic in vitro. To further advance the idea that p21 might serve as a molecular switch between senescence and transient cell-cycle arrest in response to BubR1-induced cellular stress, it will therefore be important to develop mouse models in which *p21* can be deleted in a tissue-specific and temporally control-lable fashion.

Our identification of p53 as a protector against aging-related pathology in BubR1 insufficient mice contrasts studies of other progeroid models, which have characterized p53 as an effector of functional decline (Kirkwood, 2002; Sharpless, 2004; Vousden and Lane, 2007). How can these divergent roles of p53 be reconciled? Whether p53 signaling in response to DNA damage induces apoptosis, cellular senescence, or cell-cycle arrest is highly dependent on the cell or tissue type and the nature and extent of damage (Vousden and Prives, 2009). Likewise, the various stresses implicated in the distinct progeroid models could differentially engage p53. It is conceivable that progeroid models in which p53 loss delays tissue deterioration can induce a robust p53 transcriptional response that leads to apoptosis or senescence, leading to tissue degeneration and aging. In our model, perhaps a lower chronic triggering of the p53 pathway may avoid these potentially negative effects of

cell death or senescence. Progeroid models in which p53 inactivation attenuates premature aging involve age-related features distinct from BubR1 mutant mice, raising the possibility that the tissues subjected to cellular stress are distinct, which could underlie differential consequences of p53 activation.

What might be the potential significance of our findings to natural aging? Early studies involving mutant mouse strains expressing p53 isoforms introduced the concept that p53 hyperactivity drives the aging process (Maier et al., 2004; Tyner et al., 2002). The finding that *p19*^{Arf} levels increase in many human and rodent tissues further supported this idea (Krishnamurthy et al., 2004). However, studies in normal mice subsequently suggested that p53 function actually declines with aging (Feng et al., 2007). This, together with the finding that transgenic mice containing an extra copy of wild-type endogenous *p53* and *p19*^{Arf} have an increased healthspan and lifespan (Matheu et al., 2007), has called the proaging effect of p53 into question. Our data provide in vivo support for the emerging concept that the p19^{Arf}-p53 pathway plays an important role in protection against functional decline of select tissues and organs during natural aging. It will now be important to further test this concept in naturally aged wild-type mice. It should be noted that the progeroid model used in this study may be much more relevant to normal aging than previously anticipated. In normal mice, BubR1 levels decline with aging in various tissues, with late-life BubR1 protein levels in normal mice reaching levels similar to those in *BubR1*$^{H/H}$ mice at an early age (Baker et al., 2004; Hartman et al., 2007; Matsumoto et al., 2007). Preventing this decline by sustained high overexpression of transgenic BubR1 has recently been shown to increase lifespan and healthspan of mice (Baker et al., 2013). Interestingly, attenuated sarcopenia in these mice is coupled with a delayed induction of both *p16*^{Ink4a} and *p19*^{Arf}.

EXPERIMENTAL PROCEDURES

Mouse Strains and MEFs

BubR1$^{H/H}$ mice were generated as previously described (Baker et al., 2004). *p53* (Jacks et al., 1994) and *p21* (Brugarolas et al., 1995) knockout mice were acquired from The Jackson Laboratory (Bar Harbor, ME, USA). These mice were bred to *BubR1*$^{+/H}$ mice, and the resulting double-heterozygous mice were intercrossed to generate wild-type, *BubR1*$^{H/H}$, *BubR1*$^{H/H}$;*p21*$^{-/-}$, *p21*$^{-/-}$, *BubR1*$^{H/H}$;*p53*$^{-/-}$, and *p53*$^{-/-}$ mice. Similar crosses were used to generate MEFs as previously described (Baker et al., 2008b). MEFs were generated from trypsinized carcasses of 13.5-day-old embryos as previously described (Babu et al., 2003). MEFs were cultured at 3% oxygen for two passages and then switched to 20% oxygen and used for experimentation at subsequent passages. All mice were on a mixed 129 × C57BL/6 genetic background. Animals were housed in a pathogen-free barrier environment for the duration of the study. Experimental procedures involving the use of laboratory mice were reviewed and approved by the Mayo Clinic Rochester Institutional Animal Care and Use Committee.

Western Blot Analyses

Western blot analyses were carried out as previously described (Kasper et al., 1999). Equal loading was determined using tubulin as previously described (Baker et al., 2008b). Antibodies for senescence-associated proteins were as previously described (Baker et al., 2004, 2006). Western blotting for γH2AX of 2-month-tissues was performed as previously described (Baker et al., 2008a) with Ponceau S to equalize protein loading.

Analysis of Progeroid Phenotypes

Biweekly checks for lordokyphosis and cataracts were as previously described (Baker et al., 2008b). Skeletal muscle fiber diameter measurements were performed on cross-sections of

gastrocnemius and abdominal muscles of 6-week-old male mice (n = 5 per genotype). A total of 50 fibers per sample were measured using a calibrated computer program (Olympus MicroSuite Five). Aorta thickness measurements were performed on cross-sections of paraffin-embedded aorta isolated from 2-month-old male mice (n = 5 per genotype), and 50 random-thickness measurements were taken as described above. Dissection, histology, and measurements of dermal and adipose layers of dorsal skin were performed as described previously (Baker et al., 2004). Measurements of body weight and IAT were performed on 6-week-old males (n = 5 per genotype). For analysis of cataract formation, 2-month-old eye tissue was embedded and sectioned through the middle of the lens. The number of cells that had migrated past the lens epithelial bow was counted (n = 8 lenses per genotype). Cardiotoxin treatment was performed on 2-month-old mice as previously described (Baker et al., 2008b).

qRT-PCR

qRT-PCR was performed as described on inguinal adipose tissue, skeletal muscle, and total eye tissue (Baker et al., 2008b). Lens tissue was isolated from 6-month-old mice by first removing the cornea. Both lenses of the same animal were used for RNA extraction as previously described (Baker et al., 2008b). Sequences of primers for *p16*^{Ink4a}, *p19*^{Arf}, *p21*, *Pai1*, *Igfbp2*, *IL-6*, *Mmp13*, and *Nrg1* used were as published elsewhere (Baker et al., 2011). Additionally, the following primer pairs were used: *Puma*: forward 5′-CGGACGGTCCTCAGCCCTCCCT-3′, reverse 5′-GCTCTTCTTGTCTCCG CCGCTCG-3′; *Noxa*: forward 5′-GGTGCCAGCAGACTTGAAGGACG-3′, reverse 5′-CCAATACCAGGCATTTCCATCAACC-3′; *Bid*: forward 5′-AATA GAGCCAGATTCTGAAAGTCAG-3′, reverse 5′-GCAGTTCCTTTTGTCTTCC TCCG-3′; *Bax*: forward 5′-GCTTGGGAGCGGCGGGCCCACC-3′, reverse 5′-CGATCCTGGATGAAACCCTGTAGC-3′.

In Vivo BrdU Incorporation and SA-β-Gal Staining

Analyses for in vivo BrdU incorporation were performed as previously described (Baker et al., 2008b). Adipose tissue deposits were stained for SA-β-gal activity as previously described (Baker et al., 2004). MEF growth rates and senescence staining was performed as previously described (Baker et al., 2008b).

Single-Cell Isolation, Labeling, and Collection

Preparation of single cells from inguinal adipose tissue (Baker et al., 2011) and gastrocnemius muscle (Baker et al., 2013) were as previously described. ASC, PAC, and endothelial cells were isolated from adipose tissue cell suspensions using well-documented cell-type-specific cell surface markers (Cawthorn et al., 2012). To determine the number of ASC and PAC, the total number of $CD34^{+}$;$Sca1^{+}$ cells was divided by the number of $Sca\text{-}1^{+}$ cells. Labeling and isolation of Q-SCs and FAPs was performed as described elsewhere (Joe et al., 2010). Skeletal muscle fibers were retrieved from the filter used to collect single cells after collagenase treatment. All antibodies (BD Bioscience) were used at a 1:100 dilution.

Statistical Analysis

GraphPad Prism software was used for the generation of all survival curves and for statistical analyses. Log-rank tests were used to determine overall and pairwise significance in Figures 1C, 1E, 2A, and 6A. Two-sided Wang-Allison tests were used to determine maximum lifespan changes (Wang et al., 2004) in Figure 1C. Mann-Whitney tests were used for significance in Figures 1B, 1D, 2B, 2D, 3B–3D, 6D and in Figures S1, S2A, and S2B. An unpaired t test was used for significance in Figures 4B–4D, 5A, 5B, 6C, and 6E and in

Figures S2E and S2F. For consistency in these analyses, the significance of values is defined as follows: *p < 0.05, **p < 0.01, and ***p < 0.001.

Supplementary Material

Refer to Web version on PubMed Central for supplementary material.

Acknowledgments

We thank Paul Galardy, Liviu Malureanu, Erin Hurley, Tobias Wijshake, and Robin Ricke for critical reading of the manuscript or helpful discussions. This study was supported by Ellison Medical Foundation grants (D.B. and J.v.D.), the Noaber Foundation (J.v.D), National Institutes of Health grants CA96985 and AG41122 (J.v.D.), and the Mayo Clinic Robert and Arlene Kogod Center on Aging (D.B.).

REFERENCES

Babu JR, Jeganathan KB, Baker DJ, Wu X, Kang-Decker N, van Deursen JM. Rae1 is an essential mitotic checkpoint regulator that cooperates with Bub3 to prevent chromosome missegregation. J. Cell Biol. 2003; 160:341–353. [PubMed: 12551952]

Baker DJ, Jeganathan KB, Cameron JD, Thompson M, Juneja S, Kopecka A, Kumar R, Jenkins RB, de Groen PC, Roche P, van Deursen JM. BubR1 insufficiency causes early onset of aging-associated phenotypes and infertility in mice. Nat. Genet. 2004; 36:744–749. [PubMed: 15208629]

Baker DJ, Jeganathan KB, Malureanu L, Perez-Terzic C, Terzic A, van Deursen JM. Early aging-associated phenotypes in Bub3/Rae1 haploinsufficient mice. J. Cell Biol. 2006; 172:529–540. [PubMed: 16476774]

Baker DJ, Jin F, van Deursen JM. The yin and yang of the Cdkn2a locus in senescence and aging. Cell Cycle. 2008a; 7:2795–2802. [PubMed: 18769141]

Baker DJ, Perez-Terzic C, Jin F, Pitel KS, Niederländer NJ, Jeganathan K, Yamada S, Reyes S, Rowe L, Hiddinga HJ, et al. Opposing roles for p16Ink4a and p19Arf in senescence and ageing caused by BubR1 insufficiency. Nat. Cell Biol. 2008b; 10:825–836. [PubMed: 18516091]

Baker DJ, Wijshake T, Tchkonia T, LeBrasseur NK, Childs BG, van de Sluis B, Kirkland JL, van Deursen JM. Clearance of p16Ink4a-positive senescent cells delays ageing-associated disorders. Nature. 2011; 479:232–236. [PubMed: 22048312]

Baker DJ, Dawlaty MM, Wijshake T, Jeganathan KB, Malureanu L, van Ree JH, Crespo-Diaz R, Reyes S, Seaburg L, Shapiro V, et al. Increased expression of BubR1 protects against aneuploidy and cancer and extends healthy lifespan. Nat. Cell Biol. 2013; 1:96–102. [PubMed: 23242215]

Brugarolas J, Chandrasekaran C, Gordon JI, Beach D, Jacks T, Hannon GJ. Radiation-induced cell cycle arrest compromised by p21 deficiency. Nature. 1995; 377:552–557. [PubMed: 7566157]

Burtner CR, Kennedy BK. Progeria syndromes and ageing: what is the connection? Nat. Rev. Mol. Cell Biol. 2010; 11:567–578. [PubMed: 20651707]

Campisi J. Senescent cells, tumor suppression, and organismal aging: good citizens, bad neighbors. Cell. 2005; 120:513–522. [PubMed: 15734683]

Cao L, Li W, Kim S, Brodie SG, Deng CX. Senescence, aging, and malignant transformation mediated by p53 in mice lacking the Brca1 full-length isoform. Genes Dev. 2003; 17:201–213. [PubMed: 12533509]

Cawthorn WP, Scheller EL, MacDougald OA. Adipose tissue stem cells meet preadipocyte commitment: going back to the future. J. Lipid Res. 2012; 53:227–246. [PubMed: 22140268]

Cheung TH, Quach NL, Charville GW, Liu L, Park L, Edalati A, Yoo B, Hoang P, Rando TA. Maintenance of muscle stem-cell quiescence by microRNA-489. Nature. 2012; 482:524–528. [PubMed: 22358842]

Choudhury AR, Ju Z, Djojosubroto MW, Schienke A, Lechel A, Schaetzlein S, Jiang H, Stepczynska A, Wang C, Buer J, et al. Cdkn1a deletion improves stem cell function and lifespan of mice with dysfunctional telomeres without accelerating cancer formation. Nat. Genet. 2007; 39:99–105. [PubMed: 17143283]

Conboy IM, Rando TA. The regulation of Notch signaling controls satellite cell activation and cell fate determination in postnatal myogenesis. Dev. Cell. 2002; 3:397–409. [PubMed: 12361602]

Conboy IM, Conboy MJ, Smythe GM, Rando TA. Notch-mediated restoration of regenerative potential to aged muscle. Science. 2003; 302:1575–1577. [PubMed: 14645852]

el-Deiry WS. Regulation of p53 downstream genes. Semin. Cancer Biol. 1998; 8:345–357. [PubMed: 10101800]

Feng Z, Hu W, Teresky AK, Hernando E, Cordon-Cardo C, Levine AJ. Declining p53 function in the aging process: a possible mechanism for the increased tumor incidence in older populations. Proc. Natl. Acad. Sci. USA. 2007; 104:16633–16638. [PubMed: 17921246]

Gau P, Rodriguez S, De Leonardis C, Chen P, Lin DM. Air-assisted intranasal instillation enhances adenoviral delivery to the olfactory epithelium and respiratory tract. Gene Ther. 2011; 18:432–436. [PubMed: 21085195]

Hanks S, Coleman K, Reid S, Plaja A, Firth H, Fitzpatrick D, Kidd A, Méhes K, Nash R, Robin N, et al. Constitutional aneuploidy and cancer predisposition caused by biallelic mutations in BUB1B. Nat. Genet. 2004; 36:1159–1161. [PubMed: 15475955]

Hartman TK, Wengenack TM, Poduslo JF, van Deursen JM. Mutant mice with small amounts of BubR1 display accelerated age-related gliosis. Neurobiol. Aging. 2007; 28:921–927. [PubMed: 16781018]

Jacks T, Remington L, Williams BO, Schmitt EM, Halachmi S, Bronson RT, Weinberg RA. Tumor spectrum analysis in p53-mutant mice. Curr. Biol. 1994; 4:1–7. [PubMed: 7922305]

Joe AW, Yi L, Natarajan A, Le Grand F, So L, Wang J, Rudnicki MA, Rossi FM. Muscle injury activates resident fibro/adipogenic progenitors that facilitate myogenesis. Nat. Cell Biol. 2010; 12:153–163. [PubMed: 20081841]

Kamijo T, Zindy F, Roussel MF, Quelle DE, Downing JR, Ashmun RA, Grosveld G, Sherr CJ. Tumor suppression at the mouse INK4a locus mediated by the alternative reading frame product p19ARF. Cell. 1997; 91:649–659. [PubMed: 9393858]

Kasper LH, Brindle PK, Schnabel CA, Pritchard CE, Cleary ML, van Deursen JM. CREB binding protein interacts with nucleoporin-specific FG repeats that activate transcription and mediate NUP98-HOXA9 oncogenicity. Mol. Cell. Biol. 1999; 19:764–776. [PubMed: 9858599]

Kenyon CJ. The genetics of ageing. Nature. 2010; 464:504–512. [PubMed: 20336132]

Kirkwood TB. p53 and ageing: too much of a good thing? Bioessays. 2002; 24:577–579. [PubMed: 12111716]

Krishnamurthy J, Torrice C, Ramsey MR, Kovalev GI, Al-Regaiey K, Su L, Sharpless NE. Ink4a/Arf expression is a biomarker of aging. J. Clin. Invest. 2004; 114:1299–1307. [PubMed: 15520862]

Lane AH, Aijaz N, Galvin-Parton P, Lanman J, Mangano R, Wilson TA. Mosaic variegated aneuploidy with growth hormone deficiency and congenital heart defects. Am. J. Med. Genet. 2002; 110:273–277. [PubMed: 12116237]

Lotz MK, Caramés B. Autophagy and cartilage homeostasis mechanisms in joint health, aging and OA. Nat. Rev. Rheumatol. 2011; 7:579–587. [PubMed: 21808292]

Maier B, Gluba W, Bernier B, Turner T, Mohammad K, Guise T, Sutherland A, Thorner M, Scrable H. Modulation of mammalian life span by the short isoform of p53. Genes Dev. 2004; 18:306–319. [PubMed: 14871929]

Marion RM, Strati K, Li H, Tejera A, Schoeftner S, Ortega S, Serrano M, Blasco MA. Telomeres acquire embryonic stem cell characteristics in induced pluripotent stem cells. Cell Stem Cell. 2009; 4:141–154. [PubMed: 19200803]

Matheu A, Maraver A, Klatt P, Flores I, Garcia-Cao I, Borras C, Flores JM, Viña J, Blasco MA, Serrano M. Delayed ageing through damage protection by the Arf/p53 pathway. Nature. 2007; 448:375–379. [PubMed: 17637672]

Matsumoto T, Baker DJ, d'Uscio LV, Mozammel G, Katusic ZS, van Deursen JM. Aging-associated vascular phenotype in mutant mice with low levels of BubR1. Stroke. 2007; 38:1050–1056. [PubMed: 17272762]

Matsuura S, Matsumoto Y, Morishima K, Izumi H, Matsumoto H, Ito E, Tsutsui K, Kobayashi J, Tauchi H, Kajiwara Y, et al. Monoallelic BUB1B mutations and defective mitotic-spindle

checkpoint in seven families with premature chromatid separation (PCS) syndrome. Am. J. Med. Genet. A. 2006; 140:358–367. [PubMed: 16411201]

Minagawa S, Araya J, Numata T, Nojiri S, Hara H, Yumino Y, Kawaishi M, Odaka M, Morikawa T, Nishimura SL, et al. Accelerated epithelial cell senescence in IPF and the inhibitory role of SIRT6 in TGF-β-induced senescence of human bronchial epithelial cells. Am. J. Physiol. Lung Cell. Mol. Physiol. 2011; 300:L391–L401. [PubMed: 21224216]

Nakamura Y. Isolation of p53-target genes and their functional analysis. Cancer Sci. 2004; 95:7–11. [PubMed: 14720320]

Núñez F, Chipchase MD, Clarke AR, Melton DW. Nucleotide excision repair gene (ERCC1) deficiency causes G(2) arrest in hepatocytes and a reduction in liver binucleation: the role of p53 and p21. FASEB J. 2000; 14:1073–1082. [PubMed: 10834928]

Papazoglu C, Mills AA. p53: at the crossroad between cancer and ageing. J. Pathol. 2007; 211:124–133. [PubMed: 17200941]

Rio Frio T, Lavoie J, Hamel N, Geyer FC, Kushner YB, Novak DJ, Wark L, Capelli C, Reis-Filho JS, Mai S, et al. Homozygous BUB1B mutation and susceptibility to gastrointestinal neoplasia. N. Engl. J. Med. 2010; 363:2628–2637. [PubMed: 21190457]

Sharpless NE. Ink4a/Arf links senescence and aging. Exp. Gerontol. 2004; 39:1751–1759. [PubMed: 15582292]

Suijkerbuijk SJ, van Osch MH, Bos FL, Hanks S, Rahman N, Kops GJ. Molecular causes for BUBR1 dysfunction in the human cancer predisposition syndrome mosaic variegated aneuploidy. Cancer Res. 2010; 70:4891–4900. [PubMed: 20516114]

Tyner SD, Venkatachalam S, Choi J, Jones S, Ghebranious N, Igelmann H, Lu X, Soron G, Cooper B, Brayton C, et al. p53 mutant mice that display early ageing-associated phenotypes. Nature. 2002; 415:45–53. [PubMed: 11780111]

Varela I, Cadiñanos J, Pendás AM, Gutiérrez-Fernández A, Folgueras AR, Sánchez LM, Zhou Z, Rodríguez FJ, Stewart CL, Vega JA, et al. Accelerated ageing in mice deficient in Zmpste24 protease is linked to p53 signalling activation. Nature. 2005; 437:564–568. [PubMed: 16079796]

Vousden KH, Lane DP. p53 in health and disease. Nat. Rev. Mol. Cell Biol. 2007; 8:275–283. [PubMed: 17380161]

Vousden KH, Prives C. Blinded by the Light: The Growing Complexity of p53. Cell. 2009; 137:413–431. [PubMed: 19410540]

Wang C, Li Q, Redden DT, Weindruch R, Allison DB. Statistical methods for testing effects on “maximum lifespan”. Mech. Ageing Dev. 2004; 125:629–632. [PubMed: 15491681]

Wijshake T, Malureanu LA, Baker DJ, Jeganathan KB, van de Sluis B, van Deursen JM. Reduced life- and healthspan in mice carrying a mono-allelic BubR1 MVA mutation. PLoS Genet. 2012; 8:e1003138. [PubMed: 23300461]

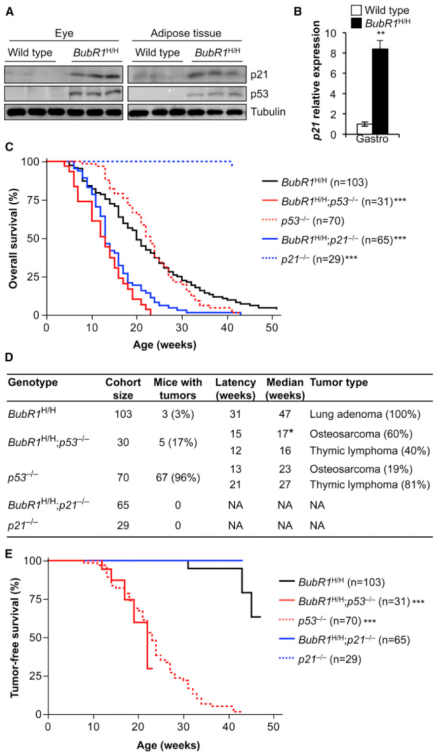

D

Genotype	Cohort size	Mice with tumors	Latency (weeks)	Median (weeks)	Tumor type
BubR1$^{H/H}$	103	3 (3%)	31	47	Lung adenoma (100%)
BubR1$^{H/H}$;*p53*$^{-/-}$	30	5 (17%)	15	17*	Osteosarcoma (60%)
			12	16	Thymic lymphoma (40%)
p53$^{-/-}$	70	67 (96%)	13	23	Osteosarcoma (19%)
			21	27	Thymic lymphoma (81%)
BubR1$^{H/H}$;*p21*$^{-/-}$	65	0	NA	NA	NA
p21$^{-/-}$	29	0	NA	NA	NA

Figure 1. p53 Promotes Longevity in BubR1 Hypomorphic Mice through *p21*

(A) Western blots of eye and adipose tissue extracts from 2-month-old wild-type and *BubR1*$^{H/H}$ mice probed with p21 and p53 antibodies. Tubulin antibody served as a loading control.

(B) qRT-PCR analysis of gastrocnemius muscles from 2-month-old mice analyzed for *p21* expression. n = 5 mice of each genotype ±SD.

(C) Kaplan-Meier overall survival curves of the indicated mice. Asterisks denote significance compared to *BubR1*$^{H/H}$ mice using log-rank tests. The maximum lifespan of *BubR1*$^{H/H}$;*p53*$^{-/-}$ and *BubR1*$^{H/H}$;*p21*$^{-/-}$ mice was significantly shortened compared to *BubR1*$^{H/H}$ mice (p = 0.0226 and p = 0.0034, respectively; two-sided Wang/Allison test referring to the proportion of mice alive at the 90th percentile survival point).

(D) Tumor incidence and latency of mice indicated in (C). The time to osteosarcoma formation in *BubR1*$^{H/H}$;*p53*$^{-/-}$ mice is significantly faster than in *p53*$^{-/-}$ mice.

(E) Tumor-free survival curves of mice dying of cancer from (C). The *BubR1*$^{H/H}$;*p53*$^{-/-}$ and *p53*$^{-/-}$ curves are both significantly different from *BubR1*$^{H/H}$ (log-rank test). No *BubR1*$^{H/H}$;*p21*$^{-/-}$ or *p21*$^{-/-}$ mice died of tumors over the duration of the experiment.

*p < 0.05; **p < 0.01; ***p < 0.001. See also Figures S1 and S2.

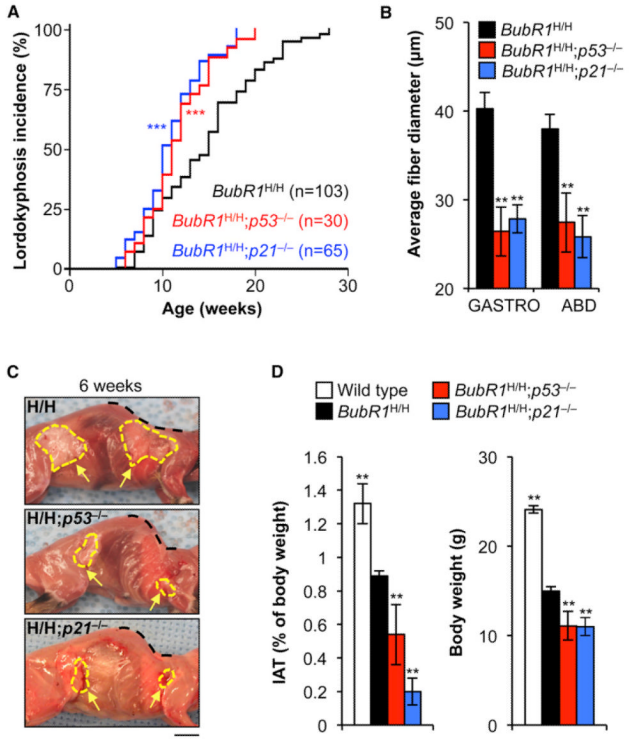

Figure 2. p53 Exerts its Antiaging Effects in Skeletal Muscle and Fat of *BubR1*$^{H/H}$ Mice through p21

(A) Incidence and latency of lordokyphosis in mice of the indicated genotypes.

(B) Average muscle fiber size of gastrocnemius and abdominal muscles of 6-week-old mice.

(C) Skinned 6-week-old *BubR1*$^{H/H}$, *BubR1*$^{H/H}$; *p53*$^{-/-}$, and *BubR1*$^{H/H}$;*p21*$^{-/-}$ mice. Note the profound lordokyphosis (black dotted line) and the markedly reduced adipose depots in the BubR1 progeroid mice lacking p53 or p21 (yellow arrows and hashed area). Scale bar represents 1 cm.

(D) IAT (left) and body weight (right) are both reduced when p53 or p21 is lost from 6-week-old BubR1 hypomorphic mice.

Data in (B) and (D) are mean ±SD (n = 5 mice per genotype). Asterisks denote significant changes from *BubR1*$^{H/H}$ values. **p < 0.01; ***p < 0.001. See also Figures S1 and S2.

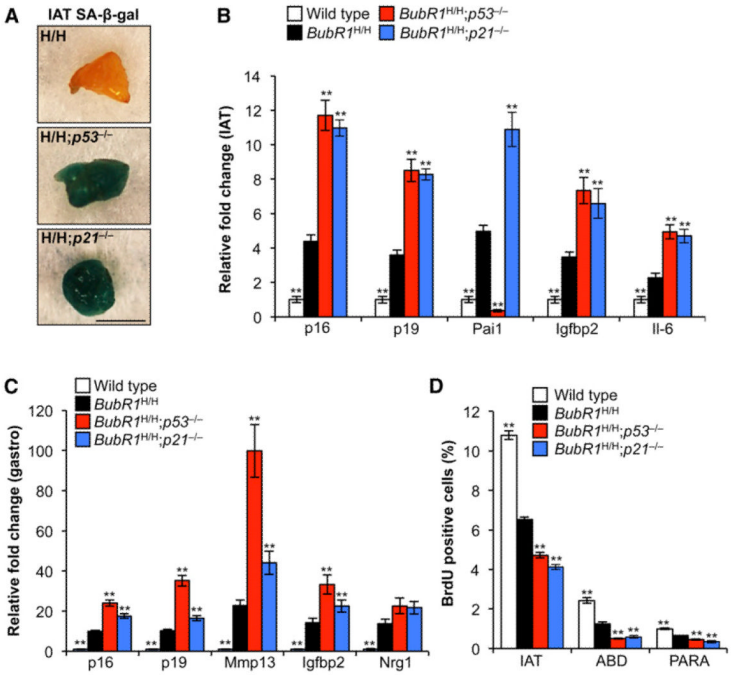

Figure 3. p53-Mediated Induction of p21 Attenuates Senescence in *BubR1*$^{H/H}$ Skeletal Muscle and fat

(A) IAT of 2-month-old *BubR1*$^{H/H}$, *BubR1*$^{H/H}$;*p53*$^{-/-}$ and *BubR1*$^{H/H}$;*p21*$^{-/-}$ mice stained for SA-β-gal activity. Scale bar, 5 mm.

(B and C) qRT-PCR analysis of senescence marker expression in IAT (B) and gastrocnemius muscles (C) of 2-month-old *BubR1*$^{H/H}$, *BubR1*$^{H/H}$;*p53*$^{-/-}$ and *BubR1*$^{H/H}$;*p21*$^{-/-}$ mice relative to wild-type mice. Values were normalized against wild-type values.

(D) Cell proliferation rates in adipose tissue and skeletal muscle of 2-month-old male mice analyzed by in vivo BrdU incorporation as a measure for in vivo senescence. ABD, abdominal muscle; PARA, paraspinal muscle.

Data in (B)–(D) are mean ±SD (n = 5 mice per genotype). Asterisks denote significant changes from *BubR1*$^{H/H}$ values. **p < 0.01. See also Figure S2.

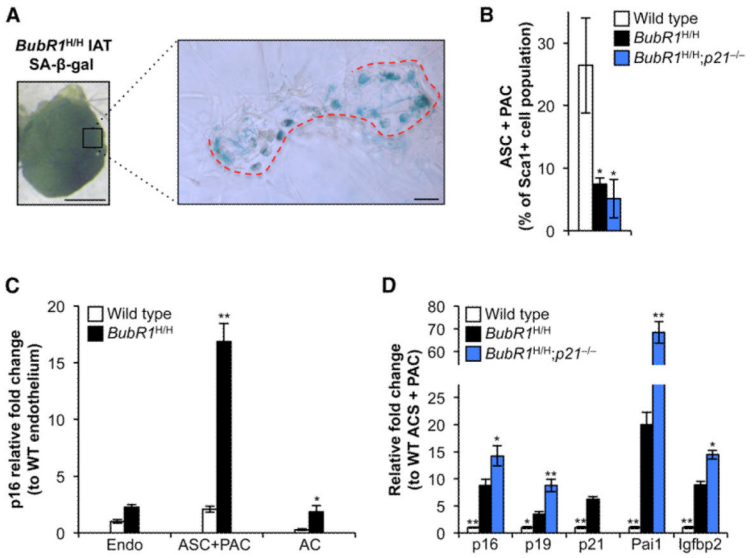

Figure 4. Fat Progenitor Cells of BubR1 Hypomorphic Mice Are Senescence Prone

(A) SA-β-gal-positive cells from IAT accumulate in regions that track along blood vessels (red dotted line) and not in mature adipocytes of 5-month-old *BubR1*$^{H/H}$ mice. Scale bars represent 1 mm (left) and 100 μm (right).

(B) Quantitation of ASCs/PACs in IAT of 2-month-old mice. Values are expressed as percent of Sca1^{+} cell numbers to account for differences in input material among genotypes.

(C) qRT-PCR analysis for *p16*^{Ink4a} expression in sorted adipose cells from 2-month-old wild-type and *BubR1*$^{H/H}$ mice. Values are normalized to wild-type endothelial cells (Endo). AC, adipocyte.

(D) qRT-PCR analysis for senescence marker expression in ASCs/PACs from 2-month-old mice relative to wild-type cells.

Data in (B)–(D) are mean ±SD (n = 3 mice per genotype). Asterisks denote significant changes from *BubR1*$^{H/H}$ values. *p < 0.05; **p < 0.01. See also Figure S3.

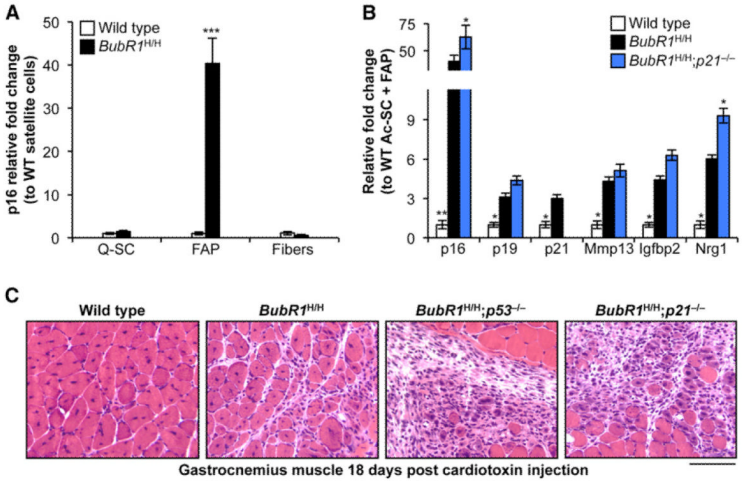

Figure 5. p21 Counteracts Progenitor Cell Senescence and Promotes Tissue Regeneration in *BubR1*$^{H/H}$ Skeletal Muscle

(A) qRT-PCR analysis for *p16*^{Ink4a} expression in sorted cells from gastrocnemius muscle of 2-month-old wild-type and *BubR1*$^{H/H}$ mice. Values are normalized to wild-type Q-SCs.

(B) qRT-PCR analysis for senescence marker expression in FAPs from 2-month-old gastrocnemius muscle. Expression is relative to wild-type cells.

(C) Gastrocnemius muscles of 2-month-old animals on day 18 after cardiotoxin injection. Note the centralized nuclei present in the myofibers of wild-type and *BubR1*$^{H/H}$ muscle, indicative of restoration of muscle architecture. In contrast, *BubR1*$^{H/H}$;*p53*$^{-/-}$ and *BubR1*$^{H/H}$;*p21*$^{-/-}$ animals have been unable to restore normal structure and still exhibit a profound hypercellular response. Scale bar represents 100 μm.

Data in (A) and (B) are mean ±SD (n = 3 mice per genotype). Asterisks denote significant changes from *BubR1*$^{H/H}$ values. *p < 0.05; **p < 0.01; ***p < 0.001. See also Figure S3.

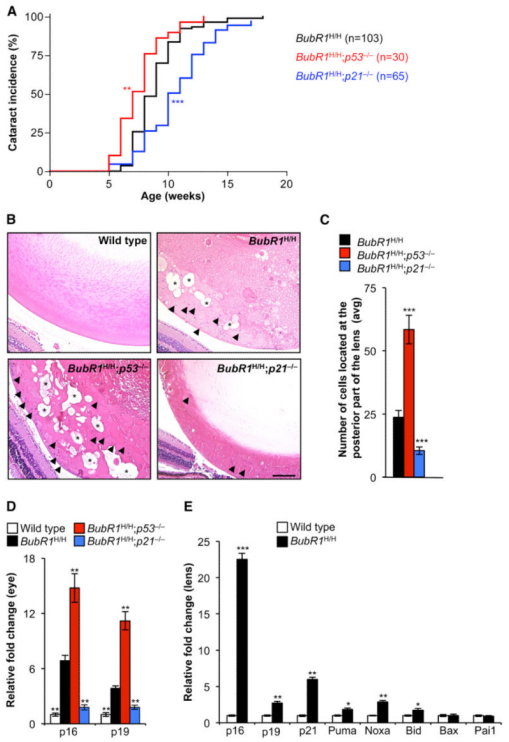

Figure 6. p53 Delays while p21 Drives Cataractogenesis in BubR1 Progeroid Mice

(A) Incidence and latency of cataract formation in *BubR1*$^{H/H}$, *BubR1*$^{H/H}$;*p53*$^{-/-}$, and *BubR1*$^{H/H}$; *p21*$^{-/-}$ animals as detected by use of slit light after dilating the eyes.

(B) Hematoxylin and eosin-stained lenses of 2-month-old mice. Arrowheads indicate posteriorly located lens epithelial cells. Asterisks mark Morgagnian globules. Scale bar represents 100 μm.

(C) Quantitation of the average number of posteriorly located cells (defined as cells that have migrated past the lens epithelial bow) in lenses of the indicated genotypes. Data are mean ±SD (n = 4 mice per genotype, two lenses per mouse). We note that no cells are detectable in this area of wild-type mice.

(D) qRT-PCR analysis of *p16*^{Ink4a} and *p19*^{Arf} expression in eye tissue of 2-month-old mice. Data are mean ±SD (n = 5 mice of each genotype). (E) qRT-PCR analysis on lens tissue of 6-month-old wild-type and *BubR1*$^{H/H}$ mice. Data are mean ±SD (n = 10 mice per genotype). Asterisks denote significant differences compared to *BubR1*$^{H/H}$ mice. *p < 0.05; **p < 0.01; ***p < 0.001. See also Figure S4.